

This work was written as part of one of the author's official duties as an Employee of the United States Government and is therefore a work of the United States Government. In accordance with 17 U.S.C. 105, no copyright protection is available for such works under U.S. Law.

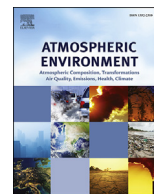
Public Domain Mark 1.0

<https://creativecommons.org/publicdomain/mark/1.0/>

Access to this work was provided by the University of Maryland, Baltimore County (UMBC) ScholarWorks@UMBC digital repository on the Maryland Shared Open Access (MD-SOAR) platform.

**Please provide feedback**

Please support the ScholarWorks@UMBC repository by emailing [scholarworks-group@umbc.edu](mailto:scholarworks-group@umbc.edu) and telling us what having access to this work means to you and why it's important to you. Thank you.



# Satellite observation of pollutant emissions from gas flaring activities near the Arctic



Can Li <sup>a, b, \*</sup>, N. Christina Hsu <sup>b</sup>, Andrew M. Sayer <sup>b, c</sup>, Nickolay A. Krotkov <sup>b</sup>, Joshua S. Fu <sup>d</sup>, Lok N. Lamsal <sup>b, c</sup>, Jaehwa Lee <sup>a, b</sup>, Si-Chee Tsay <sup>b</sup>

<sup>a</sup> Earth System Science Interdisciplinary Center, University of Maryland, College Park, MD, USA

<sup>b</sup> NASA Goddard Space Flight Center, Greenbelt, MD, USA

<sup>c</sup> Goddard Earth Sciences Technology and Research, Universities Space Research Association, Columbia, MD, USA

<sup>d</sup> Department of Civil and Environmental Engineering, University of Tennessee, Knoxville, TN, USA

## HIGHLIGHTS

- Gas flaring emissions from oil/gas fields near the Arctic studied with satellite data.
- OMI NO<sub>2</sub> data show evidence of enhanced NO<sub>x</sub> emissions due to gas flaring.
- Growth of NO<sub>2</sub> over two North American regions associated with boom in oil industry.
- Lack of significant AOD trend highlights need for longer, high-quality measurements.

## ARTICLE INFO

### Article history:

Received 29 October 2015

Received in revised form

7 March 2016

Accepted 8 March 2016

Available online 11 March 2016

### Keywords:

Gas flaring

Oil

OMI NO<sub>2</sub>

MODIS AOD

Arctic

## ABSTRACT

Gas flaring is a common practice in the oil industry that can have significant environmental impacts, but has until recently been largely overlooked in terms of relevance to climate change. We utilize data from various satellite sensors to examine pollutant emissions from oil exploitation activities in four areas near the Arctic. Despite the remoteness of these sparsely populated areas, tropospheric NO<sub>2</sub> retrieved from the Ozone Monitoring Instrument (OMI) is substantial at  $\sim 1 \times 10^{15}$  molecules cm<sup>-2</sup>, suggesting sizeable emissions from these industrial activities. Statistically significant (at the 95% confidence level, corresponding uncertainties in parentheses) increasing trends of  $0.017 (\pm 0.01) \times 10^{15}$  and  $0.015 (\pm 0.006) \times 10^{15}$  molecules cm<sup>-2</sup> year<sup>-1</sup> over 2004–2015 were found for Bakken (USA) and Athabasca (Canada), two areas having recently experienced fast expansion in the oil industry. This rapid change has implications for emission inventories, which are updated less frequently. No significant trend was found for the North Sea (Europe), where oil production has been declining since the 1990s. For northern Russia, the trend was just under the 95% significance threshold at  $0.0057 (\pm 0.006) \times 10^{15}$  molecules cm<sup>-2</sup> year<sup>-1</sup>. This raises an interesting inconsistency as prior studies have suggested that, in contrast to the continued, albeit slow, expansion of Russian oil/gas production, gas flaring in Russia has decreased in recent years. However, only a fraction of oil fields in Russia were covered in our analysis. Satellite aerosol optical depth (AOD) data revealed similar tendencies, albeit at a weaker level of statistical significance, due to the longer lifetime of aerosols and contributions from other sources. This study demonstrates that synergetic use of data from multiple satellite sensors can provide valuable information on pollutant emission sources that is otherwise difficult to acquire.

© 2016 Elsevier Ltd. All rights reserved.

## 1. Introduction

The surface temperature in the Arctic has been growing at a much greater pace than elsewhere. This Arctic amplification phenomenon (Serreze and Barry, 2011) is of particular concern, given its significant potential impacts and feedbacks to the climate

\* Corresponding author. Code 614, NASA Goddard Space Flight Center, Greenbelt, MD, USA.

E-mail address: [can.li@nasa.gov](mailto:can.li@nasa.gov) (C. Li).

system (e.g., Lawrence et al., 2008; Wang and Overland, 2009). Several physical processes, some involving short-lived atmospheric pollutants, may have contributed to the rapid warming of the Arctic (Serreze and Barry, 2011). Black carbon (BC) aerosols can warm the atmosphere by absorbing shortwave solar radiation (Shindell and Faluvegi, 2009) or by reducing the surface albedo once deposited on snow and ice (Doherty et al., 2010; Hansen and Nazarenko, 2004). Aerosol particles can also act as cloud condensation nuclei and alter the properties of Arctic clouds, causing additional warming at the surface under cloudy conditions (Garrett and Zhao, 2006; Lubin and Vogelmann, 2006).

Despite its remote location and low population density, the Arctic region has been suffering from hazy conditions since at least the 1950s (e.g., Garrett and Verzella, 2008; Shaw, 1995). The monthly mean aerosol optical depth (AOD) over the Arctic from surface-based measurements is typically less than 0.1 in summer, but can reach ~0.15 at several stations in April and May (Tomasi et al., 2015 and references therein). Long-term in situ measurements revealed similar seasonal patterns, with BC ranging between ~80–100 ng m<sup>-3</sup> in February and March and ~10 ng m<sup>-3</sup> in summer in both the European (Eleftheriadis et al., 2009) and the North American Arctic (Sharma et al., 2006). The levels of BC and other pollutant compounds (e.g., sulfate) have decreased, but remain substantial during winter/spring (e.g., Barrie, 1986; Hirdman et al., 2010; Quinn et al., 2007). A number of studies have been conducted to identify the origins of the Arctic haze. One notable source is the agricultural and forest fires in the mid-latitudes, which have contributed to some of the most severe Arctic haze events (e.g., Stohl et al., 2007). On the other hand, industrial emissions outside the Arctic Circle have been singled out as the dominant source of pollutants in the Arctic most of the time, as suggested by a number of studies involving chemical tracers (e.g., Barrie, 1986; Shaw, 1982), aircraft measurements (e.g., Jacob et al., 2010), and model simulations (e.g., Eckhardt et al., 2015; Fisher et al., 2011; Huang et al., 2014).

Another potentially important but currently understudied source of Arctic pollution is the gas flaring activities in numerous oil fields near the Arctic. Chemical transport models often underestimate BC over the Arctic and have difficulties reproducing its seasonal cycle observed in the boundary layer (e.g., Bond et al., 2013; Huang et al., 2010, 2014; Koch et al., 2009). They also tend to underestimate BC in the Arctic snow (Forsström et al., 2013). Some studies managed to improve modeling results for the Arctic by modifying the parameterization for wet and dry removal processes (e.g., Liu et al., 2011), but this may introduce biases for other regions like the Pacific (Bond et al., 2013). Using trajectory calculations and a new emission inventory that includes gas flaring emissions, Stohl et al. (2013) suggested that gas flaring could account for 42% of the annual mean surface BC in the Arctic and even more in spring. Huang et al. (2015) estimated that gas flaring made up ~30% of total BC emissions from Russia. This source, however, is currently underrepresented in most emission inventories commonly used by the modeling community.

There have been several studies on the monitoring of gas flaring activities using satellite data such as the nighttime visible light measurements from Defense Meteorological Satellite Program (DMSP, e.g., Elvidge et al., 2009) and thermal infrared measurements from the Along-Track Scanning Radiometer (ATSR) satellite sensors (Casadio et al., 2012). Field studies have also been conducted to quantify pollutant emission rate from individual gas flares (e.g., Johnson et al., 2011). However, knowledge concerning the environmental impact of gas flaring activities remains limited. The emission efficiency of trace gases and aerosols can vary from one location to another and from one moment to the next, depending on the fuel composition and combustion conditions. As

a result, quantification of air pollutants emitted from gas flares over a large area is highly uncertain. To better understand the effects of gas flaring activities on the Arctic, it is imperative to acquire more comprehensive information on their emissions and their temporal variation. In the absence of routine monitoring efforts, satellite measurements of aerosols and trace gases can be particularly useful.

While measurements of BC are presently not available from satellites, satellite NO<sub>2</sub> data may provide some insights into BC sources since both are produced in combustion and released from gas flares. Satellite NO<sub>2</sub> data have also been widely used to provide constraints on various other sources, including industry (e.g., Lamsal et al., 2011), shipping (e.g., Vinken et al., 2014), and wild fires (e.g., Mebust et al., 2011). McLinden et al. (2016) reported that satellite-observed NO<sub>2</sub> increased by 10% per year over the Canadian oil sands, in good agreement with ground monitors. In addition to NO<sub>2</sub>, AOD retrieved from satellite instruments may also provide information about the emissions of aerosols from gas flaring activities. Satellite AOD retrievals over the Arctic generally agree well with surface-based measurements particularly over the oceanic regions (Tomasi et al., 2015 and references therein), and have been used to assess the impact of fire emissions on the Arctic in some cases studies (e.g., Generoso et al., 2007). Another byproduct of gas flaring is CO, but detection of gas flaring CO emissions from satellite measurements is expected to be challenging, given its long lifetime (~30–60 days) and significant natural sources. In this study, we attempt to characterize pollutants over some major oil fields near the Arctic, using NO<sub>2</sub> and AOD retrievals from a suite of satellite sensors.

## 2. Data and methodology

### 2.1. Satellite and auxiliary datasets

Two satellite retrieval products are used in the present study: tropospheric column NO<sub>2</sub> from the Ozone Monitoring Instrument (OMI) aboard the Aura spacecraft, and total vertical columnar aerosol optical depth (AOD) from the Moderate Resolution Imaging Spectroradiometer (MODIS) aboard Aqua. The study period is from 2004 to 2015, corresponding to the Aura mission to date (Aqua was launched in 2002). Note that results are quantitatively similar if MODIS Terra data (launched in 2000) are used instead of Aqua. We also use the updated NASA 'Black Marble' image (cf. <http://earthobservatory.nasa.gov/NaturalHazards/view.php?id=79803>), created from nighttime measurements from the day-night band (DNB) of the Visible Infrared Imaging Radiometer Suite (VIIRS) sensor aboard the Suomi National Polar-orbiting Partnership (NPP) satellite launched in October 2011 (Liao et al., 2013). This 'Black Marble' is used only in an illustrative (qualitative) sense, to show spatial patterns of night lights related to human activities. Night lights from residential/industrial anthropogenic activities are generally persistent features, and so identification of locations affected by gas flaring should not be significantly affected by the time period chosen for the DNB composite. Other studies (e.g., Elvidge et al., 2009, 2013) have used Operational Linescan System (OLS) and DNB data in a quantitative sense to examine industrial activities, but here we use NO<sub>2</sub> and AOD as proxies to take a deliberately different approach.

For NO<sub>2</sub>, the latest version 2.1 NASA standard OMI tropospheric NO<sub>2</sub> data product (Bucsela et al., 2013; Lamsal et al., 2014) was used. The level 2 NO<sub>2</sub> retrievals have a nominal spatial resolution of 13 × 24 km<sup>2</sup> at nadir. Pixels with cloud radiance fraction <0.5 and considered to have good retrieval quality were selected to generate a daily level 3 dataset at 0.25° × 0.25° resolution. Since 2007, the OMI instrument has been experiencing a partial field of view

blockage problem known as the row anomaly that severely affects the radiance measurements from a portion of its 60 cross-track scan positions. To minimize the impact of row anomaly on our data analysis, we only used OMI data from scan positions 5–23, which were unaffected by the row anomaly throughout the entire study period. This also ensures consistency in data sampling for the trend analysis in this study.

For aerosols, the latest MODIS Aqua Collection 6 data product was used. Daily composites of AOD at 550 nm averaged to  $1^\circ \times 1^\circ$  horizontal resolution were used (no gridded product at a resolution equivalent to OMI is available). Over land, the enhanced Deep Blue data set (Hsu et al., 2013) is used, which has been validated and found to be stable over the Aqua mission to date (Sayer et al., 2013, 2014), while over water the Dark Target ocean data set (Levy et al., 2013) is used. In both cases, AOD at 550 nm over land and ocean is retrieved from daytime MODIS measurements at a nominal ground resolution of  $10 \times 10 \text{ km}^2$ .

The analyses for both of these satellite products are restricted to data from May to October, as during boreal winter months coverage at these high northern latitudes is sparse or absent entirely, because of snow, ice, or polar night. This leads to potential retrieval artifacts and sampling limitations in the data. In contrast, the May–October period has fairly complete spatial coverage at the relevant areas of interest.

In addition to satellite products, we also examined the estimated emissions of  $\text{NO}_x$  for the year 2008 in the Emissions Database for Global Atmospheric Research (EDGAR) HTAP V2 inventory (available at [http://edgar.jrc.ec.europa.eu/htap\\_v2/index.php?SECURE=123](http://edgar.jrc.ec.europa.eu/htap_v2/index.php?SECURE=123), Janssens-Maenhout et al., 2015). The EDGAR HTAP emission inventory provides total emissions, as well as sector-by-sector estimates (for air, energy, industry, residential, shipping, and transportation sectors), and is used in this study as an example to demonstrate how emissions related to gas flaring activities are represented in typical regional/global inventories. Additional use of population density data from the Gridded Population of the World (GPW) version 3 data set (available at <http://sedac.ciesin.columbia.edu/data/collection/gpw-v3>) allows for comparison with Black Marble images to identify areas of industrial development (e.g., nighttime light sources in unpopulated areas).

## 2.2. Data analysis

The daily gridded AOD and tropospheric  $\text{NO}_2$  datasets were aggregated to calculate the monthly median value for each grid cell, and only grid cells with at least 3 (for  $\text{NO}_2$ ) and 5 (for AOD) days contributing to the monthly median were considered for further analysis. The use of medians rather than means highlights the persistent background levels, as medians are less sensitive than means to outliers, and the higher threshold of number of days for AOD was selected to eliminate poorly-sampled months when available days were influenced significantly by wildfires. Extreme atmospheric events are likely to cause large positive outliers and skew the mean and affect hotspot/trend detection (e.g., Carn and Lopez, 2011; Chubarova et al., 2012). Our analysis focuses on four selected regions known for gas and oil exploitation activities: the North Sea ( $56.75\text{--}62^\circ\text{N}$ ,  $0\text{--}3.75^\circ\text{E}$ ); Bakken ( $47.25\text{--}49^\circ\text{N}$ ,  $102\text{--}104^\circ\text{W}$ ); Athabasca ( $56\text{--}58^\circ\text{N}$ ,  $110\text{--}113^\circ\text{W}$ ); and northern Russia ( $62\text{--}67^\circ\text{N}$ ,  $71\text{--}80^\circ\text{E}$ ). These domains are shown in Fig. 1a. Note that this northern Russian region comprises parts of several major oil fields in the western Siberian region; some of these fields are still in the early stage of commercial exploitation, with only pilot activities, while others have been in operation for a longer time.

Trends were then calculated for these four regions from the monthly median fields by taking the spatial mean of the gridded

data (from May to October each year) over each region, and creating a time series. The winter months were excluded due to limitations as described in section 2.1. Some areas, northern Russia in particular, may see substantial influence from biomass burning in summer months, although this is mitigated through the use of monthly medians rather than means. However, for the AOD analysis, August 2007 was excluded from Bakken, and August–September 2010 from Northern Russia, as these months were otherwise strong outliers (even in monthly median) due to strong wildfires (e.g., Chubarova et al., 2012).

For  $\text{NO}_2$ , the Black Marble image and EDGAR HTAP inventory were further used to subset pixels within the larger regions, to distinguish areas dominated by gas flaring emissions. Only grid cells having a high level of gas flaring activities and small emissions from other sources were included in the trend calculations. Note that this may cause a decreasing trend to be underestimated, if gas flaring or oil production ceased in part of the oil fields prior to the EDGAR HTAP inventory/VIIRS measurements. On the other hand, this should not affect the detection of any increase in pollutant emissions due to the expansion of oil fields. For this particular study, oil production remained relatively stable or became greater in most of our selected areas, with North Sea being the only exception. As a test for the method, we also calculated the trends for the four areas without excluding any grid cells and the results were qualitatively consistent.

Next, the tropospheric  $\text{NO}_2$  time series was converted to anomaly time series by deseasonalizing the data (i.e., subtracting the mean May tropospheric  $\text{NO}_2$  column from all May data in that region, and so forth for the other months). Then, least-squares linear regression on the anomaly time series was used to calculate the trend, with each time series point's uncertainty taken as the standard error on the regional monthly average value. Trends were estimated to be statistically significant at the 95% confidence level if the magnitude of the trend per year (i.e. linear fit gradient) was greater than twice the standard deviation of the residuals on the linear fit. There are more sophisticated methods for refining trend uncertainty, such as accounting for the autocorrelation in the time series using the fit residuals (e.g., Weatherhead et al., 1998). This method was not used here due to the gaps in the time series (November–April data) that will result in uncertainties in the estimates of autocorrelation. Due to the short lifetime of  $\text{NO}_2$  (e.g., Valin et al., 2013), however,  $\text{NO}_2$  residual autocorrelation is expected to be small.

The same analysis was conducted for the MODIS AOD data, although due to the coarser data spatial resolution compared to the other data sets, the calculation was done over the whole area rather than only the subset of pixels where gas flaring emissions were thought to be dominant.

## 3. Results and discussion

### 3.1. Study regions, emission inventories, and oil/gas production

Fig. 1 provides an overview of our study regions. As can be seen from the figure, the spatial distribution of nighttime lights (Fig. 1a) is on a broad scale consistent with that of the population density (Fig. 1b). The highly populated urbanized areas in eastern North America, Europe, and eastern China can all be identified as hotspots in Fig. 1a. As expected, these areas also have the strongest  $\text{NO}_x$  emissions (Fig. 1c) according to the EDGAR emission inventory (Janssens-Maenhout et al., 2015). Although not shown here,  $\text{SO}_2$  emissions are also in general stronger in areas with large population density, particularly China due to the country's reliance on coal as the predominant source of energy and less stringent pollution control measures (e.g., Li et al., 2010). It is worth mentioning that

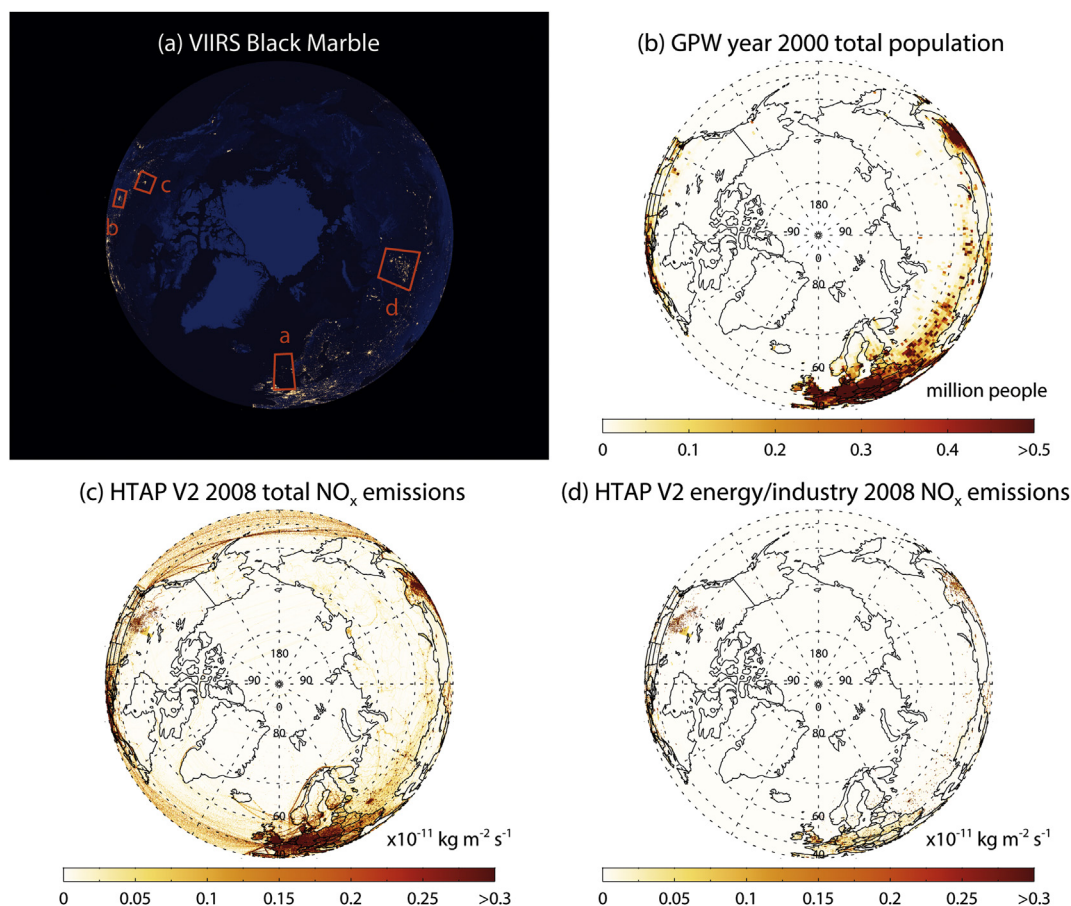


**Fig. 1.** (a) VIIRS 'Black Marble' image composite of Day Night Band (DNB) measurements of nighttime light signals over northern hemisphere mid/high-latitudes, (b) GPW population density for the same region for the year 2000, estimated NO<sub>x</sub> emissions for the same region for year 2008 in the EDGAR HTAP V2 emission inventory for (c) all sectors and (d) only the energy and industrial sectors. Red boxes in (a) define the four areas with oil exploitation activities that are the focus of the study. (For interpretation of the references to colour in this figure legend, the reader is referred to the web version of this article.)

emissions of SO<sub>2</sub> and NO<sub>x</sub> are not entirely co-located, as they are emitted from different processes (see Krotkov et al., 2015 for more details). For example, some of the large SO<sub>2</sub> point sources such as smelters in Norilsk, Russia are located in remote mining areas with relatively small NO<sub>x</sub> emissions. Several areas marked with red boxes in Fig. 1a have fairly strong lights at night but much smaller population density. One thing in common between these areas is that they all have substantial gas and oil exploitation activities. The light signals present in the Black Marble image over these areas are due to gas flares and other industrial activities in the oil fields. The estimated pollutant emissions for the areas in the EDGAR HTAP inventory are sizable for North Sea and Athabasca (Areas a and c in Fig. 1a), but negligible for Bakken and northern Russia (Areas b and d in the same figure). If only the industrial and energy sectors in the EDGAR HTAP inventory are considered, the emissions for those four areas are even less (Fig. 1d).

Fig. 2 presents estimates of the annual crude oil and natural gas production in these four regions since the year 2000. These come from a variety of sources. For the North Sea, direct estimates are not readily available, so offshore UK production estimates from the United States Energy Information Administration (EIA), available from <http://www.eia.gov/beta/international/>, are used instead. Although some of the oil and gas production in this area is Norwegian, the bulk of the study region is in the British sector, and so this data may be taken as a proxy for North Sea production, at least for the temporal trends we are concerned with. Production records

for Bakken are available from the North Dakota Industrial Commission at <https://www.dmr.nd.gov/oilgas/> and used here. Data for Athabasca are not readily available, although oil production data for the province of Alberta as a whole (for which Athabasca is the major component) are available from Statistics Canada at <http://www5.statcan.gc.ca/cansim/> (CANSIM table 126-0001). Gas production is not available from that source. Finally, Russian production data are also available from the US EIA, and although not broken down on a regional level, the temporal behaviour of production can be taken as a proxy for that of the western Siberian fields contained within the Northern Russia region. Note that geographically-distant regions such as Sakhalin Island also contribute to the total production estimates in Fig. 2.

Where both oil and gas data are available, the two tend to increase or decrease in concert. UK offshore production shows a roughly linear decline, falling by more than a factor of two since the year 2000. In contrast, both Bakken and Alberta show increasing production, becoming more rapid since approximately 2008. Russia dwarfs the other regions in terms of total output, although the relative pace of change is smaller (a slow increase). It is a relevant question as to whether these diverse changes in regional production translate to different trends in emissions, which would ideally need to be accounted for in emission inventories such as EDGAR HTAP and others. All other things being equal this would be expected to be the case, although changes in the quality of oil/gas being extracted, improvements in technologies, and other factors

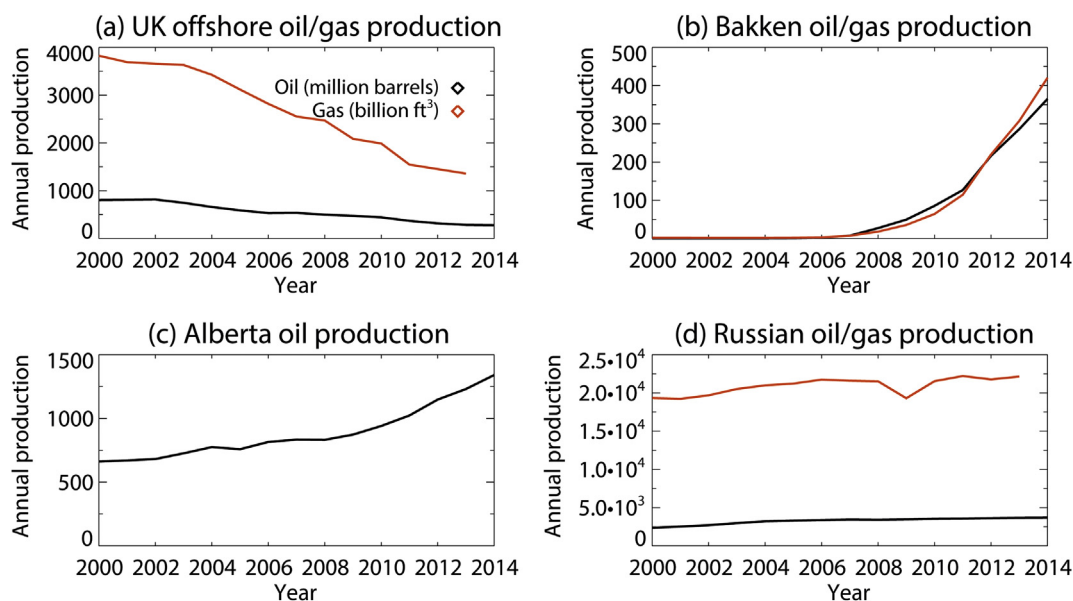


**Fig. 2.** Annual crude oil (black) and dry natural gas (red) production estimates for the four regions highlighted in Fig. 1, or larger regions enclosing them. (For interpretation of the references to colour in this figure legend, the reader is referred to the web version of this article.)

such as accidents could all influence the effective emissions per unit production. For example, despite the increase in production in Russia, observational studies based on night light detection suggest that gas flaring activities in Russia have declined during the 21st century (Elvidge et al., 2009; Casadio et al., 2012). The OMI and MODIS retrievals provide tools to take an independent look at this problem.

### 3.2. Satellite observations of tropospheric $\text{NO}_2$ and AOD

Hemispheric maps of tropospheric  $\text{NO}_2$  and AOD levels are shown in Figs. 3 and 4, respectively. Qualitatively, OMI  $\text{NO}_2$  hotspots show a similar spatial distribution to hotspots in the emission inventory. For AOD this is less clear-cut, due to the contributions from a wide range of emission sources and secondary production (e.g., other industrial emissions, as well as wildfire smoke and maritime aerosol, among others) to total AOD in these regions. By comparing the spatial patterns of median  $\text{NO}_2$  and AOD in the first (2004–2009) and second (2010–2015) halves of the Aura mission to date, the basic patterns remain in most cases the same, although there are some spatially-coherent areas of increase or decrease.

A closer look at the available data for the four areas of interest is provided in Fig. 5. The EDGAR HTAP estimates of  $\text{NO}_x$  sources in the North Sea area (Fig. 5i) indicate contributions from shipping, although when these sectors are removed (Fig. 5m) distinct signals from the oil rigs (also visible as lights in the Black Marble) become more visible. The agreement between the inventory and the night lights may be attributed to the fact that the oil fields in the North Sea have been operational for a few decades, and their environmental impacts are relatively well known. The gas flaring signals are not as distinguishable in the satellite tropospheric  $\text{NO}_2$  or AOD (Fig. 5q and u), probably due to transport from nearby areas over land. The weak enhancement of OMI-retrieved tropospheric  $\text{NO}_2$  over areas with oil rigs suggests that the retrieval may capture emissions from gas flaring. This is not the case for AOD here, likely because of the maritime and continental contributions to the signal; the typical background AOD for the Atlantic Ocean at these latitudes is around 0.05–0.15 (e.g., Smirnov et al., 2011) so gas flaring is likely too weak to make a detectable contribution.

The Bakken area in North Dakota (USA) is also sparsely populated (Fig. 5f). Oil production from Bakken was relatively small until 2008, but has since been growing exponentially (Fig. 2 and Mason,

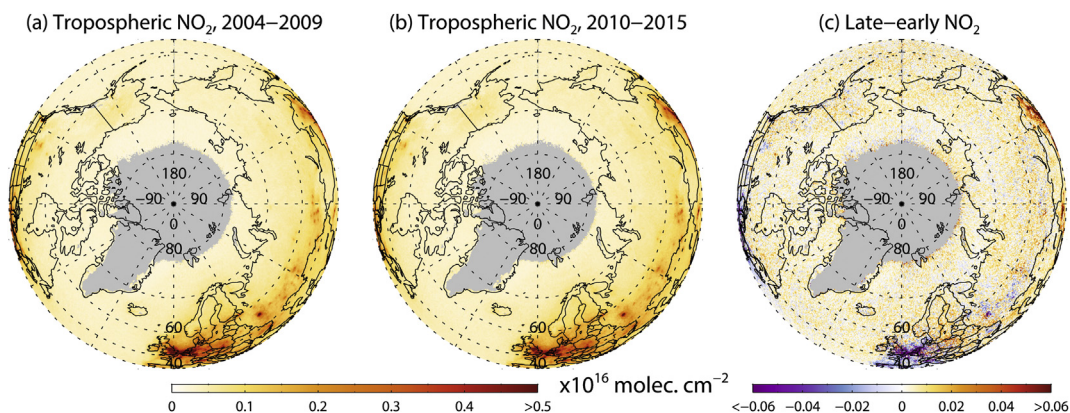


**Fig. 3.** May–October median tropospheric  $\text{NO}_2$  from OMI, for (a) 2004–2009, (b) 2010–2015, and (c) the difference between these two periods.

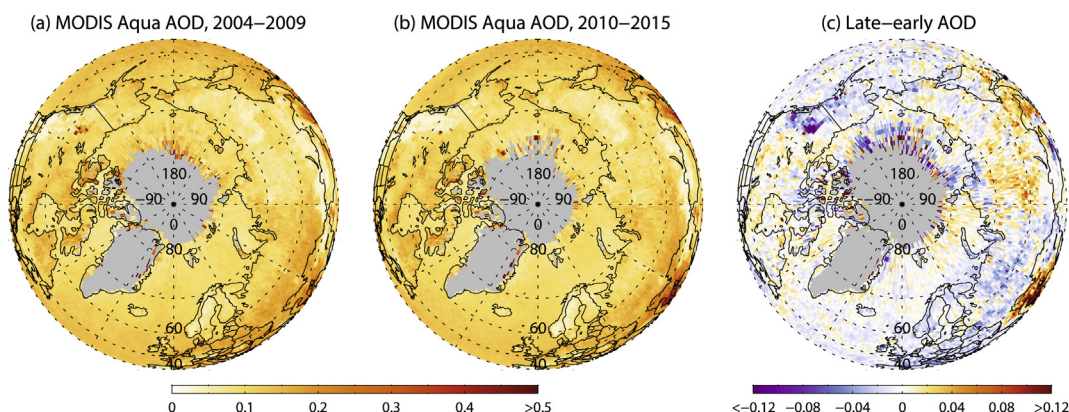


Fig. 4. Same as Fig. 3, except for MODIS Aqua AOD, using Deep Blue over land and Dark Target ocean over water.

2012). The bulk of the EDGAR HTAP emissions in the area, however, are from the residential and transportation sectors, with little contribution from energy/industry. The OMI and MODIS 2004–2015 records do not detect hot spots in this area (in the case of MODIS, the data resolution is coarse compared to the study region), which may in part reflect the weak production for the first half of the data record. Note that the large signal to the immediate southeast of the region corresponds to the location of the Cold Creek power plant, online since 1979, and this may wash out any smaller hotspot in the OMI data (although again does not yield a hotspot in MODIS AOD).

For the Athabasca area in Alberta (Canada), the estimated emissions in the EDGAR HTAP inventory (Fig. 5k and o) include contributions from not only residential and transportation sectors, but also the oil industry. One may notice that there is a mismatch between the light signals (Fig. 5c) and the emission inventory (Fig. 5o) in the primary oil exploitation zone, with the most of the estimated emissions located to the south of the majority of visible gas flares. The OMI tropospheric  $\text{NO}_2$  (Fig. 5o and s), on the other hand, is consistent with the night lights data and points to greater loading near the center of the dotted box. The box-like shape of part of the EDGAR HTAP inventory in this region likely reflects a lack of knowledge about the precise location of some of the emissions. Again, the AOD data do not appear to be able to identify these hot spots.

Compared to Bakken and Athabasca, the gas flares in the northern Russian oil fields are scattered over a vast area (Fig. 5d). While the region is also generally sparsely populated (Fig. 5h), it also features nearby cities like Surgut (61.15°N, 73.26°E) and some of the largest oil-fired power plants in the world (i.e., Surgut-1 and -2 Power Stations), visible to the south of the studied area in both the EDGAR HTAP inventories (Fig. 5i and p) as well as OMI  $\text{NO}_2$  (Fig. 5t). Inside the blue box, the enhancement in tropospheric  $\text{NO}_2$  due to gas flaring is not as obvious as in the cases of Bakken and Athabasca (Fig. 5p and t). Still, there appears to be some spatial correspondence.

In brief, the above analysis suggests that the OMI tropospheric  $\text{NO}_2$  data generally show the ability to capture stationary sources from gas flaring activities. In contrast, the satellite AOD products, at least at the available horizontal grid size of  $1^\circ$ , are not able to do so, likely also due to contributions from other sources to the aerosol burden.

### 3.3. Changes in tropospheric $\text{NO}_2$ and column AOD over high-latitude oil fields in the last decade

Figs. 6 and 7 present time-series of OMI tropospheric  $\text{NO}_2$  and

MODIS AOD, respectively, over our identified oil exploitation zones near the Arctic. As mentioned previously, to focus on the contribution from gas flaring activities, monthly median values were calculated for each grid cell and then regional mean values were calculated from these. Because of the seasonality inherent in both data sets, deseasonalized summertime (May–October) data were used to derive linear trends.

No statistically significant trend was detected in the mean OMI tropospheric  $\text{NO}_2$  over the oil fields in North Sea for the period of 2004–2015. Although oil production in the area has been declining since the 1990s, contributions from other sectors may be masking any signal. For Bakken, our determined linear trend over the last decade is  $0.017 (\pm 0.005) \times 10^{15} \text{ molecules cm}^{-2} \text{ year}^{-1}$  (hereafter numbers in parentheses indicate the one-standard-deviation (68%) confidence interval of the trend), which is significant at the 95% confidence level. A closer examination indicates that the  $\text{NO}_2$  loading was relatively stable until 2009, which is consistent with the increasing pace of oil/gas production in this region (Fig. 2). A similar upward trend of  $0.015 (\pm 0.003) \times 10^{15} \text{ molecules cm}^{-2} \text{ year}^{-1}$  is found for Athabasca, in agreement with the analysis by McLinden et al. (2012, 2014, 2016) revealing strong growth in  $\text{NO}_x$  emissions in the area due to exploitation of Alberta tar sands, and again consistent with Fig. 2.

For northern Russia, the trend in  $\text{NO}_2$  loading over oil fields is not statistically different from zero at the 95% confidence level, at  $0.0057 (\pm 0.003) \times 10^{15} \text{ molecules cm}^{-2} \text{ year}^{-1}$ . This is at odds with the recent assertion that gas flaring activities in Russia are in decline (e.g., Casadio et al., 2012; Elvidge et al., 2009), although those studies were based on nighttime light measurements rather than retrievals of pollutant concentrations. Additionally, it should be noted that our study only covers a fraction of all the oil fields in Russia, so it is not clear how representative either the aforementioned studies or the production estimates in Fig. 2 are of activity in our study region. The monthly anomalies also indicate an increase from 2004 to 2010 and a decrease from 2010 onwards. A linear trend model may not realistically reflect the actual changes in oil/gas production in the area. Finally, the lack of significant trend in the present study may also be attributed to the delay in the implementation of the original plan to reduce gas flaring emissions in Russia (Z. Klimont, personal communication).

For both the North Sea and northern Russia, the AOD trends are not significantly different from zero, and are much smaller than their trend uncertainties. For the trend to be statistically significant at a 95% confidence level, the rate of AOD change needs to exceed 0.02 per decade over the North Sea and 0.04 over northern Russia. AOD changes of similar or greater magnitudes have been detected in many other places of the globe (e.g., Hsu et al., 2012), so the lack of a detected

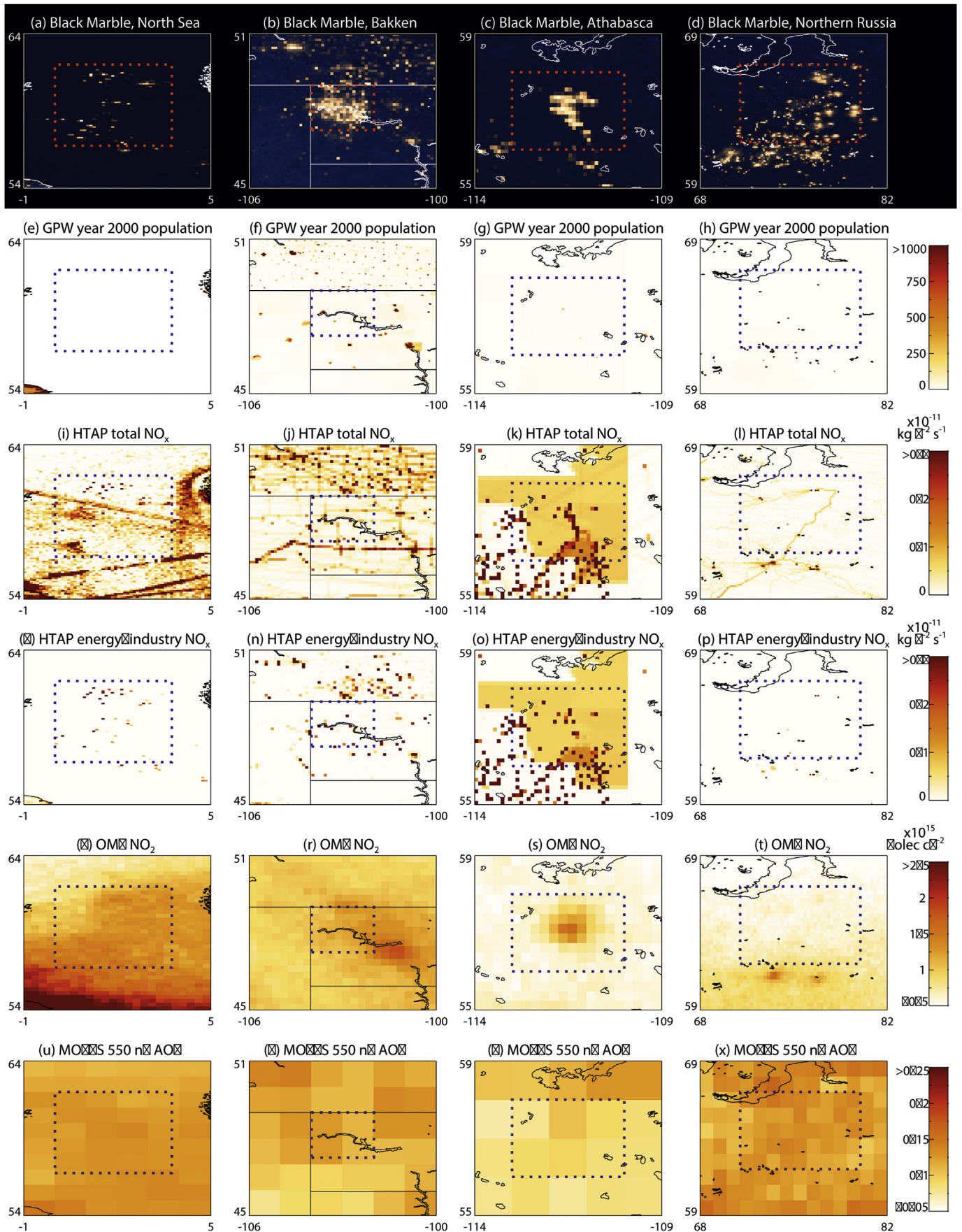


**Fig. 5.** Overview of the four regions (from left-right, columns show the North Sea, Bakken, Athabasca, and Northern Russia) highlighted in Fig. 1. From top to bottom, panels show the VIIRS Black Marble image; GPW total population for the year 2000; EDGAR HTAP V2 total and energy/industrial  $\text{NO}_x$  emissions, median OMI tropospheric  $\text{NO}_2$  for May–October 2004–2015, and median MODIS Aqua AOD at 550 nm for the same period. Dotted boxes represent zones designated for trend analysis (cf. Fig. 6 and 7).

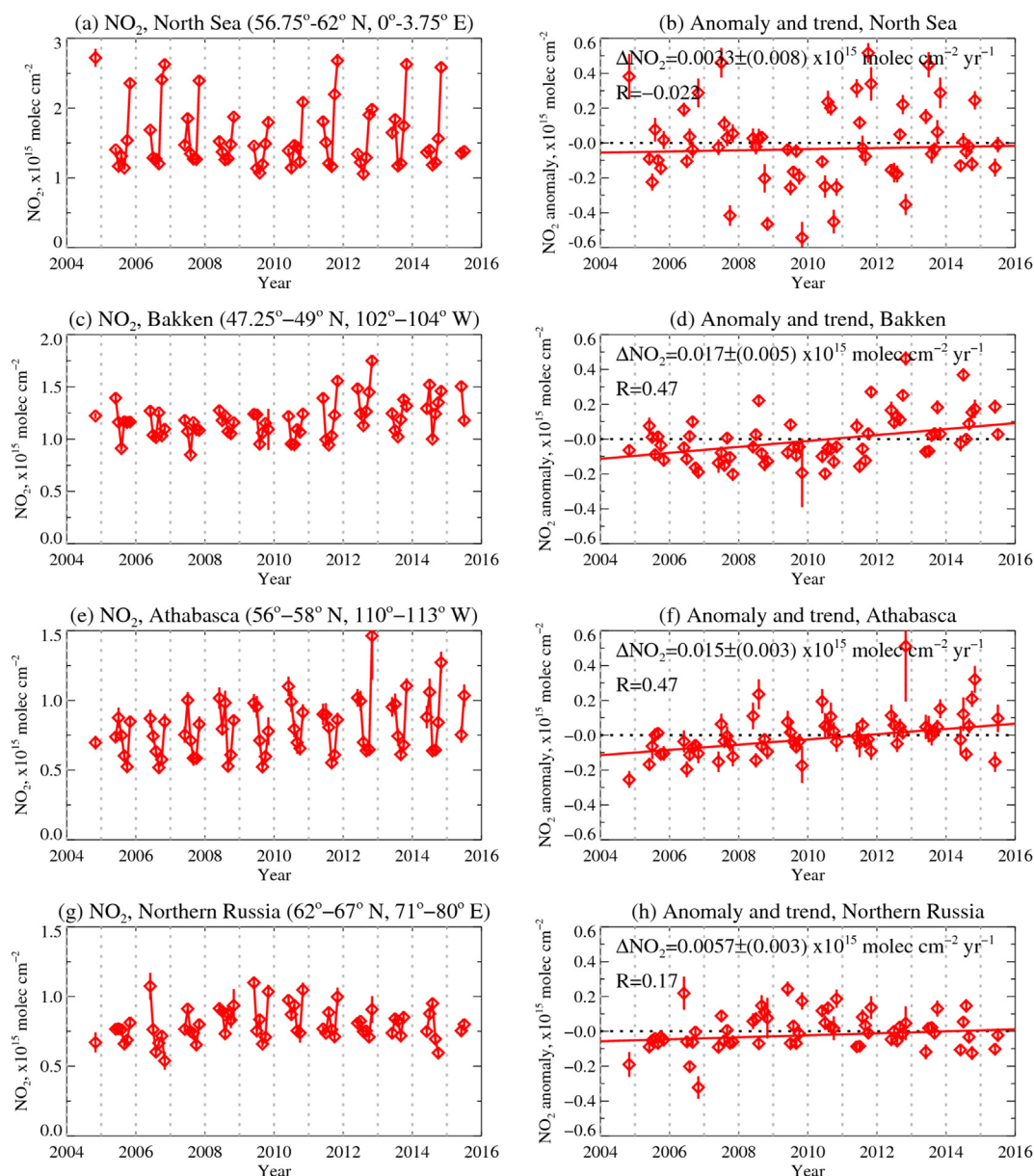


**Fig. 6.** Left: time series of monthly mean OMI tropospheric  $\text{NO}_2$  over (a) North Sea, (c) Bakken, (e) Athabasca, and (g) northern Russia. Right: monthly deseasonalized  $\text{NO}_2$  anomalies. In both columns, error bars indicate the standard error in the box-average monthly  $\text{NO}_2$  column. Red lines represent the derived linear trends for the four areas. Linear correlation coefficient, trend magnitude, and the 68% (one standard deviation) confidence interval of the linear trends are also given for each area. Dashed grey lines separate each year. (For interpretation of the references to colour in this figure legend, the reader is referred to the web version of this article.)

trend in the AOD is evidence that any trend in these areas, particularly resulting from potential changes in oil/gas flaring activities, has been negligible over the past decade. It may be that changes in the productivity of these oil fields (Fig. 2) are not reflected in changing emissions of aerosols. Bakken and Athabasca exhibit AOD trends that are qualitatively consistent with those in  $\text{NO}_2$  and oil field production, but only at approximately 90% confidence level. The contribution of other local and transported aerosol sources is likely in part the reason for the weaker trends, even with median filtering of the data, as in summertime boreal North America is often influenced by large biomass burning smokes.

#### 4. Conclusions and perspective

In summary, we analyzed measurements from the OMI and MODIS sensors, with additional context provided by VIIRS DNB

night lights (the ‘Black Marble’), population density, and  $\text{NO}_x$  emission inventory data to examine pollutant emissions from gas flaring activities in four major oil exploitation areas near the Arctic. The results demonstrate that OMI in particular can provide useful information on pollutant emissions from gas flaring activities, which can supplement other analyses based on night lights. While not analyzed in this study, the intensity of gas flares can also be observed using DMS-OLS and the VIIRS DNB and may allow pollutant emissions to be parameterized, if ground-truth measurements are available for developing such a parameterization (e.g., Elvidge et al., 2009). For remote regions with industrial activities leading to relatively isolated hotspots (e.g., Bakken and Athabasca), satellite retrievals of tropospheric  $\text{NO}_2$  could potentially be used to enhance these efforts.

Aerosols tend to have a longer lifetime and more complicated sources. And it is difficult to directly link retrieved AOD to gas

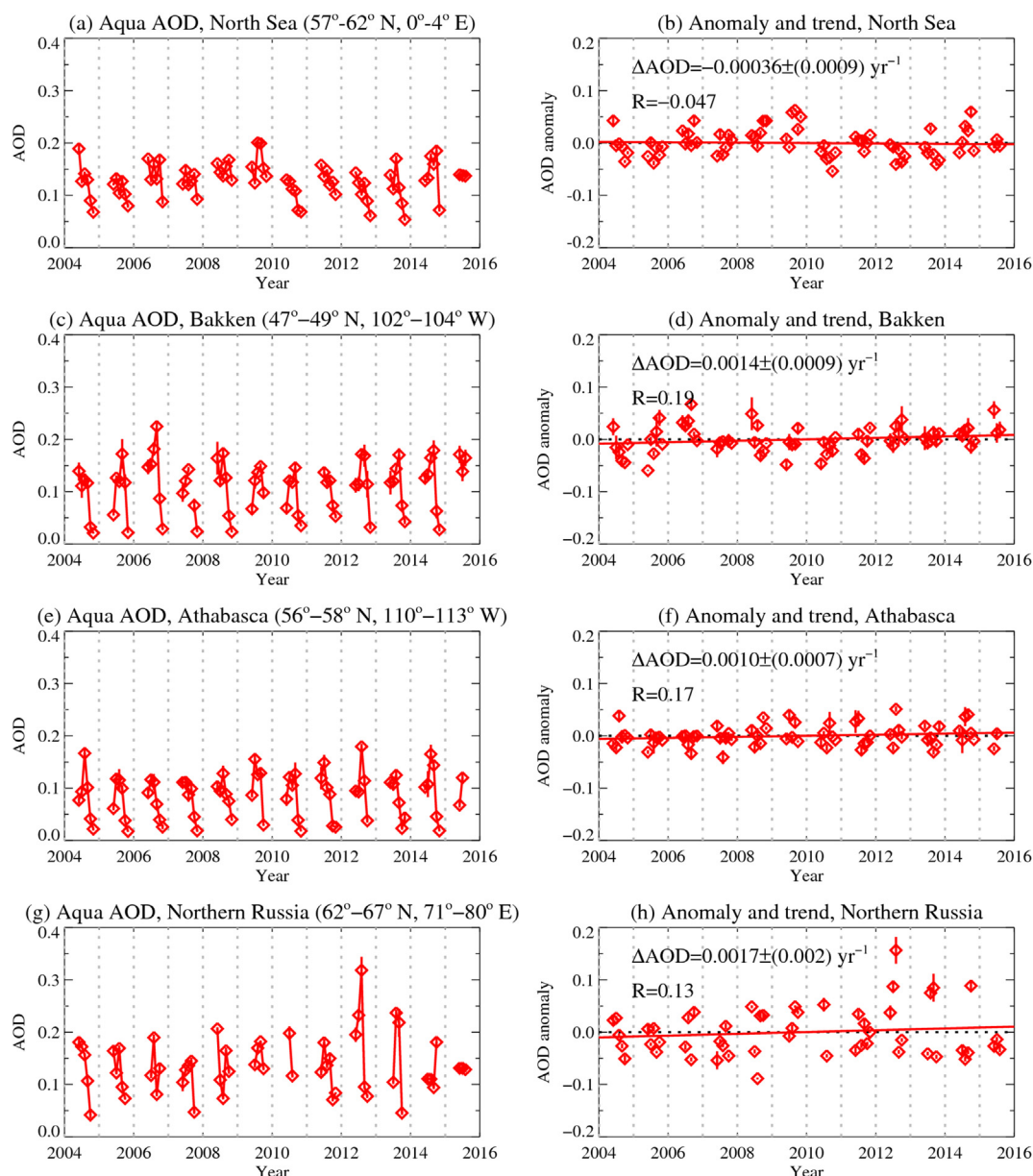


Fig. 7. Same as Fig. 6, except for MODIS Aqua AOD.

flaring emissions. While satellite-based AOD trend analyses (e.g., Hsu et al., 2012) can reveal the presence or absence of trends in aerosol loading with fidelity, efforts such as the present study and the model-based analysis of Chin et al. (2014) illustrate the complementary nature of using multiple data sets together to tease out the reasons for the observed trends.

Like many other efforts attempting to apply satellite data in studying air quality and atmospheric chemistry, there are also several limitations in this study. The oil fields investigated here are all located at relatively high latitudes and can have significant environmental impacts given their proximity to the Arctic. However, solar/satellite geometries, surface conditions, and cloudiness in these regions are often not ideal for retrievals of AOD or  $\text{NO}_2$ , which may lead to greater uncertainties compared with retrievals in other parts of the world. It is critical to develop capabilities that will improve satellite measurements of gaseous pollutants and aerosols over the areas in and around the Arctic. Additionally, the

emissions from some oil fields are smaller and can be difficult to detect using satellites. Future instruments such as TROPOMI (TROPOspheric Monitoring Instrument, Veeffkind et al., 2012), and TEMPO (Tropospheric Emissions: Monitoring of POLLution, Chance et al., 2013) that will offer greater resolution may help to improve sensitivity to these smaller sources. Finally, more quantitative estimates of the environmental effects of gas flaring can be obtained, once satellite data are ingested into chemical transport and climate models. Such applications will undoubtedly benefit from improved satellite retrievals with smaller and well-understood uncertainties.

## Acknowledgements

The authors wish to thank Robert Simmon (formerly of NASA Earth Observatory at NASA GSFC) for the 'Black Marble' VIIRS Day-Night Band composite. The OMI standard  $\text{NO}_2$  product is funded by NASA Earth Sciences Division, and are archived and can be obtained

free of charge at the Goddard Earth Sciences (GES) Data and Information Services Center (DISC, <http://daac.gsfc.nasa.gov/>). The MODIS aerosol products are funded under the NASA Earth Observing System (EOS) program, managed by Hal Maring, and are archived and can be obtained free of charge from <http://ladsweb.nascom.nasa.gov/>. The Center for International Earth Science Information Network at Columbia University and Centro Internacional de Agricultura Tropical are thanked for the GPW data, and EU Joint Research Council (JRC) thanked for the EDGAR HTAP V2 emission inventory. <http://ladsweb.nascom.nasa.gov>.

## References

- Barrie, L.A., 1986. Arctic air pollution: an overview of current knowledge. *Atmos. Environ.* 20, 643–663.
- Bond, T.C., Doherty, S.J., Fahey, D.W., Forster, P.M., Bernsten, T., DeAngelo, B.J., Flanner, M.G., Ghan, S., Kärcher, B., Koch, D., Kinne, S., Kondo, Y., Quinn, P.K., Sarofim, M.C., Schultz, M.G., Schulz, M., Venkataraman, C., Zhang, H., Zhang, S., Bellouin, N., Guttikunda, S.K., Hopke, P.K., Jacobson, M.Z., Kaiser, J.W., Klimont, Z., Lohmann, U., Schwarz, J.P., Shindell, D., Storelvmo, T., Warren, S.G., Zender, C.S., 2013. Bounding the role of black carbon in the climate system: a scientific assessment. *J. Geophys. Res. Atmos.* 118, 5380–5552. <http://dx.doi.org/10.1002/jgrd.50171>.
- Bucsela, E.J., Krotkov, N.A., Celarier, E.A., Lamsal, L.N., Swartz, W.H., Bhartia, P.K., Boersma, K.F., Veefkind, J.P., Gleason, J.F., Pickering, K.E., 2013. A new stratospheric and tropospheric NO<sub>2</sub> retrieval algorithm for nadir-viewing satellite instruments: applications to OMI. *Atmos. Meas. Tech.* 6, 2607–2626. <http://dx.doi.org/10.5194/amt-6-2607-2013>.
- Casadio, S., Arino, O., Serpe, D., 2012. Gas flaring monitoring from space using the ATSR instrument series. *Remote Sens. Environ.* 116, 239–249.
- Carn, S.A., Lopez, T.M., 2011. Opportunistic validation of sulfur dioxide in the Sarychev Peak volcanic eruption cloud. *Atmos. Meas. Tech.* 4, 1705–1712. <http://dx.doi.org/10.5194/amt-4-1705-2011>.
- Chance, K., Liu, X., Suleiman, R.M., Flittner, D.E., Al-Saadi, J., Janz, S.J., 2013. Tropospheric emissions: monitoring of pollution (TEMPO). In: Butler, J.J., Xiong, X., Gu, X. (Eds.), *Proceedings of SPIE, Earth Observing Systems XVIII*. 88660D. SPIE – International Society for Optical Engineering. <http://dx.doi.org/10.1117/12.024479>.
- Chin, M., Diehl, T., Tan, Q., Prospero, J.M., Kahn, R.A., Remer, L.A., Yu, H., Sayer, A.M., Bian, H., Geogdzhayev, I.V., Holben, B.N., Howell, S.G., Huebert, B.J., Hsu, N.C., Kim, D., Kucsera, T.L., Levy, R.C., Mishchenko, M.I., Pan, X., Quinn, P.K., Schuster, G.L., Streets, D.G., Stroe, S.A., Torres, O., Zhao, X.-P., 2014. Multi-decadal aerosol variations from 1980 to 2009: a perspective from observations and a global model. *Atmos. Chem. Phys.* 14, 3657–3690. <http://dx.doi.org/10.5194/acp-14-3657-2014>.
- Chubarova, N., Nezval, Y., Sviridenkov, I., Smirnov, A., Slutsker, I., 2012. Smoke aerosol and its radiative effects during extreme fire event over Central Russia in summer 2010. *Atmos. Meas. Tech.* 5, 557–568. <http://dx.doi.org/10.5194/amt-5-557-2012>.
- Doherty, S.J., Warren, S.G., Grenfell, T.C., Clarke, A.D., Brandt, R.E., 2010. Light-absorbing impurities in Arctic snow. *Atmos. Chem. Phys.* 10, 11647–11680.
- Eckhardt, S., Quennehen, B., Olivié, D.J.L., Bernsten, T.K., Cherian, R., Christensen, J.H., Collins, W., Crepinsek, S., Daskalakis, N., Flanner, M., Herber, A., Heyes, C., Hodnebrog, Ø., Huang, L., Kanakidou, M., Klimont, Z., Langner, J., Law, K.S., Lund, M.T., Mahmood, R., Massling, A., Myriokefalitakis, S., Nielsen, I.E., Nøjgaard, J.K., Quaas, J., Quinn, P.K., Raut, J.-C., Rumbold, S.T., Schulz, M., Sharma, S., Skeie, R.B., Skov, H., Uttal, T., von Salzen, K., Stohl, A., 2015. Current model capabilities for simulating black carbon and sulfate concentrations in the Arctic atmosphere: a multi-model evaluation using a comprehensive measurement data set. *Atmos. Chem. Phys.* 15, 9413–9433. <http://dx.doi.org/10.5194/acp-15-9413-2015>.
- Eleftheriadis, K., Vratolis, S., Nyeki, S., 2009. Aerosol black carbon in the European Arctic: measurements at Zeppelin station, Ny-Ålesund, Svalbard from 1998–2007. *Geophys. Res. Lett.* 36, L02809. <http://dx.doi.org/10.1029/2008GL035741>.
- Elvidge, C.D., Ziskin, D., Baugh, K.E., Tuttle, B.T., Ghosh, T., Pack, D.W., Erwin, E.H., Zhizhin, M., 2009. A fifteen year record of global natural gas flaring derived from satellite data. *Energies* 2, 595–622. <http://dx.doi.org/10.3390/en20300595>.
- Elvidge, C.D., Zhizhin, M., Hsu, F.-C., Baugh, K.E., 2013. VIIRS nightfire: satellite pyrometry at night. *Remote Sens.* 5, 4423–4449. <http://dx.doi.org/10.3390/rs5094423>.
- Fisher, J.A., Jacob, D.J., Wang, Q., Bahreini, R., Carouge, C.C., Cubison, M.J., Dibb, J.E., Diehl, T., Jimenez, J.L., Leibenberger, E.M., Meinders, M.B.J., Pye, H.O.T., Quinn, P.K., Sharma, S., van Donkelaar, A., Yantosca, R.M., 2011. Sources, distribution, and acidity of sulfate-ammonium aerosol in the Arctic in winter-spring. *Atmos. Environ.* 45, 7301–7318.
- Forsström, S., Isaksson, E., Skeie, R.B., Ström, J., Pedersen, C.A., Hudson, S.R., Bernsten, T.K., Lihavainen, H., Godtlieden, F., Gerland, S., 2013. Elemental carbon measurements in European Arctic snow packs. *J. Geophys. Res. Atmos.* 118 <http://dx.doi.org/10.1002/2013JD019886>.
- Garrett, T.J., Verzella, L.L., 2008. Looking back: an evolving history of Arctic aerosols. *Bull. Am. Meteorol. Soc.* 89, 299–302.
- Garrett, T.J., Zhao, C., 2006. Increased Arctic cloud longwave emissivity associated with pollution from mid-latitudes. *Nature* 440, 787–789.
- Generoso, S., Bey, I., Attié, J.-L., Bréon, F.-M., 2007. A satellite- and model-based assessment of the 2003 Russian fires: impact on the Arctic region. *J. Geophys. Res.* 112, D15302. <http://dx.doi.org/10.1029/2006JD008344>.
- Hansen, J., Nazarenko, L., 2004. Soot climate forcing via snow and ice albedo. *Proc. Natl. Acad. Sci.* 101, 423–428.
- Hirdman, D., Burkhardt, J.F., Sodemann, H., Eckhardt, S., Jefferson, A., Quinn, P.K., Sharma, S., Ström, J., Stohl, A., 2010. Long-term trends of black carbon and sulfate aerosol in the Arctic: changes in atmospheric transport and source region emissions. *Atmos. Chem. Phys.* 10, 9351–9368.
- Hsu, N.C., Gautam, R., Sayer, A.M., Bettenhausen, C., Li, C., Jeong, M.J., Tsay, S.-C., Holben, B.N., 2012. Global and regional trends of aerosol optical depth over land and ocean using SeaWiFS measurements from 1997 to 2010. *Atmos. Chem. Phys.* 12, 8037–8053. <http://dx.doi.org/10.5194/acp-12-8037-2012>.
- Hsu, N.C., Jeong, M.-J., Bettenhausen, C., Sayer, A.M., Hansell, R., Seftor, C.S., Huang, J., Tsay, S.-C., 2013. Enhanced Deep Blue aerosol retrieval algorithm: the second generation. *J. Geophys. Res. Atmos.* 118, 9296–9315. <http://dx.doi.org/10.1002/jgrd.50712>.
- Huang, K., Fu, J.S., Hodson, E.L., Dong, X., Cresko, J., Prikhodko, V.Y., Storey, J.M., Cheng, M.-D., 2014. Identification of missing anthropogenic emission sources in Russia: implication for modeling Arctic haze. *Aerosol Air Qual. Res.* 14, 1799–1811. <http://dx.doi.org/10.4209/aaqr.2014.08.0165>.
- Huang, K., Fu, J.S., Prikhodko, V.Y., Storey, J.M., Romanov, A., Hodson, E.L., Cresko, J., Morozova, I., Ignatieva, Y., Cabaniss, J., 2015. Russian anthropogenic black carbon: emission reconstruction and Arctic black carbon simulation. *J. Geophys. Res. Atmos.* 120 <http://dx.doi.org/10.1002/2015JD023358>.
- Huang, L., Gong, S.L., Jia, C.Q., Lavoue, D., 2010. Importance of deposition process in simulating the seasonality of the Arctic black carbon aerosol. *J. Geophys. Res. Atmos.* 115, D17207. <http://dx.doi.org/10.1029/2009JD013478>.
- Jacob, D.J., Crawford, J.H., Maring, H., Clarke, A.D., Dibb, J.E., Emmons, L.K., Ferrare, R.A., Hostetler, C.A., Russell, P.B., Singh, H.B., Thompson, A.M., Shaw, G.E., McCauley, E., Pederson, J.R., Fisher, J.A., 2010. The Arctic research of the composition of the troposphere from aircraft and satellites (ARCTAS) mission: design, execution, and first results. *Atmos. Chem. Phys.* 10, 5191–5212.
- Janssens-Maenhout, G., Crippa, M., Guizzardi, D., Dentener, F., Muntean, M., Pouliot, G., Keating, T., Zhang, Q., Kurokawa, J., Wankmüller, R., Denier van der Gon, H., Kuenen, J.J.P., Klimont, Z., Frost, G., Darras, S., Koffi, B., Li, M., 2015. HTAP.v2.2: a mosaic of regional and global emission grid maps for 2008 and 2010 to study hemispheric transport of air pollution. *Atmos. Chem. Phys.* 15, 11411–11432. <http://dx.doi.org/10.5194/acp-15-11411-2015>.
- Johnson, M.R., Devillers, R.W., Thomson, K.A., 2011. Quantitative field measurement of soot emission from a large gas flare using sky-LOSA. *Environ. Sci. Technol.* 45, 345–350.
- Koch, D., Schulz, M., Kinne, S., McNaughton, C., Spackman, J.R., Balkanski, Y., Bauer, S., Bernsten, T., Bond, T.C., Boucher, O., Chin, M., Clarke, A., De Luca, N., Dentener, F., Diehl, T., Dubovik, O., Easter, R., Fahey, D.W., Feichter, J., Fillmore, D., Freitag, S., Ghan, S., Ginoux, P., Gong, S., Horowitz, L., Iversen, T., Kirkevåg, A., Klimont, Z., Kondo, Y., Krol, M., Liu, X., Miller, R., Montanaro, V., Moteki, N., Myhre, G., Penner, J.E., Perlwitz, J., Pitari, G., Reddy, S., Sahu, L., Sakamoto, H., Schuster, G., Schwarz, J.P., Seland, Ø., Stier, P., Takegawa, N., Takemura, T., Textor, C., van Aardenne, J.A., Zhao, Y., 2009. Evaluation of black carbon estimations in global aerosol models. *Atmos. Chem. Phys.* 9, 9001–9026.
- Krotkov, N.A., McLinden, C.A., Li, C., Lamsal, L.N., Celarier, E.A., Marchenko, S.V., Swartz, W.H., Bucsela, E.J., Joiner, J., Duncan, B.N., Boersma, K.F., Veefkind, J.P., Levelt, P.F., Fioletov, V.E., Dickerson, R.R., He, H., Lu, Z., Streets, D.G., 2015. Aura OMI observations of regional SO<sub>2</sub> and NO<sub>2</sub> pollution changes from 2005 to 2014. *Atmos. Chem. Phys. Discuss.* 15, 26555–26607. <http://dx.doi.org/10.5194/acpd-15-26555-2015>.
- Lamsal, L.N., Martin, R.V., Padmanabhan, A., van Donkelaar, A., Zhang, Q., Sioris, C.E., Chance, K., Kurosu, T.P., Newchurch, M.J., 2011. Application of satellite observations for timely updates to global anthropogenic NO<sub>x</sub> emission inventories. *Geophys. Res. Lett.* 38, L05810. <http://dx.doi.org/10.1029/2010GL046476>.
- Lamsal, L.N., Krotkov, N.A., Celarier, E.A., Swartz, W.H., Pickering, K.E., Bucsela, E.J., Gleason, J.F., Martin, R.V., Philip, S., Irie, H., Cede, A., Herman, J., Weinheimer, A., Szykman, J.J., Knepp, T.N., 2014. Evaluation of OMI operational standard NO<sub>2</sub> column retrievals using in situ and surface-based NO<sub>2</sub> observations. *Atmos. Chem. Phys.* 14, 11587–11609. <http://dx.doi.org/10.5194/acp-14-11587-2014>.
- Lawrence, D.M., Slater, A.G., Tomas, R.A., Holland, M.M., Deser, C., 2008. Accelerated Arctic land warming and permafrost degradation during rapid sea ice loss. *Geophys. Res. Lett.* 35, L1506. <http://dx.doi.org/10.1029/2008GL033894>.
- Levy, R.C., Mattoo, S., Munchak, L.A., Remer, L.A., Sayer, A.M., Patadia, F., Hsu, N.C., 2013. The Collection 6 MODIS aerosol products over land and ocean. *Atmos. Meas. Tech.* 6, 2989–3034. <http://dx.doi.org/10.5194/amt-6-2989-2013>.
- Li, C., Zhang, Q., Krotkov, N.A., Streets, D.G., He, K., Tsay, S.-C., Gleason, J.F., 2010. Recent large reduction in sulfur dioxide emissions from Chinese power plants observed by the Ozone Monitoring Instrument. *Geophys. Res. Lett.* 37, L08807. <http://dx.doi.org/10.1029/2010GL042594>.
- Liao, L.B., Weiss, S., Mills, S., Hauss, B., 2013. Suomi NPP VIIRS day-night band on-orbit performance. *J. Geophys. Res. Atmos.* 118, 12705–12718. <http://dx.doi.org/10.1002/2013JD020475>.
- Liu, J., Fan, S., Horowitz, L.W., Levy II, H., 2011. Evaluation of factors controlling long-range-transport of black carbon to the Arctic. *J. Geophys. Res. Atmos.* 116,

- D04307. <http://dx.doi.org/10.1029/2010JD015145>.
- Lubin, D., Vogelmann, A.M., 2006. A climatologically significant aerosol longwave indirect effect in Arctic. *Nature* 439, 453–456.
- Mason, J., 2012. Bakken's maximum potential oil production rate explored. *Oil Gas J.* 110, 76–86.
- McLinden, C.A., Fioletov, V., Boersma, K.F., Krotkov, N., Sioris, C.E., Veefkind, J.P., Yang, K., 2012. Air quality over the Canadian oil sands: a first assessment using satellite observations. *Geophys. Res. Lett.* 39, L04804. <http://dx.doi.org/10.1029/2011GL050273>.
- McLinden, C.A., Fioletov, V., Boersma, K.F., Kharol, S.K., Krotkov, N., Lamsal, L., Makar, P.A., Martin, R.V., Veefkind, J.P., Yang, K., 2014. Improved satellite retrievals of NO<sub>2</sub> and SO<sub>2</sub> over the Canadian oil sands and comparisons with surface measurements. *Atmos. Chem. Phys.* 14, 3637–3656. <http://dx.doi.org/10.5194/acp-14-3637-2014>.
- McLinden, C.A., Fioletov, V., Krotkov, N.A., Li, C., Boersma, K.F., Adams, C., 2016. A decade of change in NO<sub>2</sub> and SO<sub>2</sub> over the Canadian oil sands as seen from space. *Environ. Sci. Technol.* 50, 331–337. <http://dx.doi.org/10.1021/acs.est.5b04985>.
- Meibust, A.K., Russell, A.R., Hudman, R.C., Valin, L.C., Cohen, R.C., 2011. Characterization of wildfire NO<sub>x</sub> emissions using MODIS fire radiative power and OMI tropospheric NO<sub>2</sub> columns. *Atmos. Chem. Phys.* 11, 5839–5851.
- Quinn, P.K., Shaw, G., Andrews, E., Dutton, E.G., Ruoho-Airola, T., Gong, S.L., 2007. Arctic haze: current trends and knowledge gaps. *Tellus* 59B, 99–114.
- Sayer, A.M., Hsu, N.C., Bettenhausen, C., Jeong, M.-J., 2013. Validation and uncertainty estimates for MODIS Collection 6 "Deep Blue" aerosol data. *J. Geophys. Res. Atmos.* 118, 7864–7872. <http://dx.doi.org/10.1002/jgrd.50600>.
- Sayer, A.M., Munchak, L.A., Hsu, N.C., Levy, R.C., Bettenhausen, C., Jeong, M.-J., 2014. MODIS Collection 6 aerosol products: comparison between Aqua's e-Deep Blue, Dark Target, and "merged" data sets, and usage recommendations. *J. Geophys. Res. Atmos.* 119, 13965–13989. <http://dx.doi.org/10.1002/2014JD022453>.
- Serreze, M.C., Barry, R.G., 2011. Processes and impacts of Arctic amplification: a research synthesis. *Glob. Planet. Change* 77, 85–96.
- Sharma, S., Andrews, E., Barrie, L.A., Ogren, J.A., Lavoué, D., 2006. Variations and sources of the equivalent black carbon in the high Arctic revealed by long-term observations at Alert and Barrow: 1989–2003. *J. Geophys. Res. Atmos.* 111, D14208. <http://dx.doi.org/10.1029/2005JD006581>.
- Shaw, G.E., 1982. Evidence for a central Eurasian source of Arctic haze in Alaska. *Nature* 299, 815–818.
- Shaw, G.E., 1995. The Arctic haze phenomenon. *Bull. Am. Meteorol. Soc.* 76, 2403–2413.
- Shindell, D., Faluvegi, G., 2009. Climate response to regional radiative forcing during the twentieth century. *Nat. Geosci.* 2, 294–300. <http://dx.doi.org/10.1038/NGE0473>.
- Smirnov, A., Holben, B.N., Giles, D.M., Slutsker, I., O'Neill, N.T., Eck, T.F., Macke, A., Croot, P., Courcoux, Y., Sakerin, S.M., Smyth, T.J., Zielinski, T., Zibordi, G., Goes, J.I., Harvey, M.J., Quinn, P.K., Nelson, N.B., Radionov, V.F., Duarte, C.M., Losno, R., Sciare, J., Voss, K.J., Kinne, S., Nalli, N.R., Joseph, E., Krishna Moorthy, K., Covert, D.S., Gulev, S.K., Milinevsky, G., Larouche, P., Belanger, S., Horne, E., Chin, M., Remer, L.A., Kahn, R.A., Reid, J.S., Schulz, M., Heald, C.L., Zhang, J., Lapina, K., Kleidman, R.G., Griesfeller, J., Gaitley, B.J., Tan, Q., Diehl, T.L., 2011. Maritime aerosol network as a component of AERONET – first results and comparison with global aerosol models and satellite retrievals. *Atmos. Meas. Tech.* 4, 583–597. <http://dx.doi.org/10.5194/amt-4-583-2011>.
- Stohl, A., Berg, T., Burkhardt, J.F., Fjærraa, A.M., Forster, C., Herber, A., Hov, Ø., Lunder, C., McMillan, W.W., Oltmans, S., Shiobara, M., Simpson, D., Solberg, S., Stebel, K., Ström, J., Tørseth, K., Treffeisen, R., Virkkunen, K., Yttri, K.E., 2007. Arctic smoke – record high air pollution levels in the European Arctic due to agricultural fires in Eastern Europe in spring 2006. *Atmos. Chem. Phys.* 7, 511–534.
- Stohl, A., Klimont, Z., Eckhardt, S., Kupiainen, K., Shevchenko, V.P., Kopeikin, V.M., Novigatsky, A.N., 2013. Black carbon in the Arctic: the underestimated role of gas flaring and residential combustion emissions. *Atmos. Chem. Phys.* 13, 8833–8855.
- Tomasi, C., Kokhanovsky, A.A., Lupi, A., Ritter, C., Smirnov, A., O'Neill, N.T., Stone, R.S., Holben, B.N., Nyeki, S., Wehrli, C., Stohl, A., Mazzola, M., Lanconelli, C., Vitale, V., Stebel, K., Aaltonen, A., de Leeuw, G., Rodriguez, E., Herber, A.B., Radionov, V.F., Zielinski, T., Petelski, T., Sakerin, S.M., Kabanov, D.M., Xue, Y., Mei, L., Istomina, L., Wagener, R., McArthur, B., Sobolewski, P.S., Kivi, R., Courcoux, Y., Larouche, P., Broccardo, S., Piketh, S.J., 2015. Aerosol remote sensing in polar regions. *Earth Sci. Rev.* 140, 108–157.
- Valin, L.C., Russell, A.R., Cohen, R.C., 2013. Variations of OH radical in an urban plume inferred from NO<sub>2</sub> column measurements. *Geophys. Res. Lett.* 40, 1856–1860. <http://dx.doi.org/10.1002/grl.50267>.
- Veefkind, J.P., Aben, I., McMullan, K., Forster, H., de Vries, J., Otter, G., Claas, J., Eskes, H.J., de Haan, J.F., Kleipool, Q., van Weele, M., Hasekamp, O., Hoogeveen, R., Landgraf, J., Snel, R., Tol, P., Ingmann, P., Voors, R., Kruizinga, B., Vink, R., Visser, H., Levelt, P.F., 2012. TROPOMI on the ESA Sentinel-5 Precursor: a GMES mission for global observations of the atmospheric composition for climate, air quality and ozone layer applications. *Remote Sens. Environ.* 120, 70–83. <http://dx.doi.org/10.1016/j.rse.2011.09.027>.
- Vinken, G.C.M., Boersma, K.F., van Donkelaar, A., Zhang, L., 2014. Constraints on ship NO<sub>x</sub> emissions in Europe using GEOS-Chem and OMI satellite NO<sub>2</sub> observations. *Atmos. Chem. Phys.* 14, 1353–1369.
- Wang, M., Overland, J.E., 2009. A sea ice free summer Arctic within 30 years? *Geophys. Res. Lett.* 36, L07502. <http://dx.doi.org/10.1029/2009GL037820>.
- Weatherhead, E.C., Reinsel, G.C., Tiao, G.C., Meng, X.-L., Choi, D., Cheang, W.-K., Keller, T., DeLuise, J., Wuebbles, D.J., Kerr, J.B., Miller, A.J., Oltmans, S.J., Frederick, J.E., 1998. Factors affecting the detection of trends: statistical considerations and applications to environmental data. *J. Geophys. Res. Atmos.* 103, 17149–17161. <http://dx.doi.org/10.1029/98JD00995>.